Interactions of 77Se and 13CO with nickel in the active site of active F420- non-reducing hydrogenase from Methanococcus voltae.

Sorgenfrei, O.; Duin, E.L.; Klein, A.; Albracht, S.P.J.

Published in:
The Journal of Biological Chemistry

THE JOURNAL OF BIOLOGICAL CHEMISTRY
Vol. 271, No. 39, Issue of September 27, pp. 23799–23806, 1996

Printed in U.S.A.

Interactions of ^{77}Se and ^{13}CO with Nickel in the Active Site of Active F_{420}-nonreducing Hydrogenase from *Methanococcus voltae**

(Received for publication, April 5, 1996, and in revised form, June 17, 1996)

Oliver Sorgenfrei‡§, Evert C. Duin¶, Albrecht Klein‡, and Simon P. J. Albracht¶

From ‡Molecular Genetics, Department of Biology, University of Marburg, Karl-von-Frisch-Strasse, D-35032 Marburg/Lahn, Germany and ¶E. C. Slater Institute, BioCentrum Amsterdam, Plantage Muidergracht 12, NL-1018 TV Amsterdam, The Netherlands

The selenium-containing F_{420}-nonreducing hydrogenase from *Methanococcus voltae* was prepared in the Ni_a(I)·CO state. The effect of illumination on this light-sensitive species was studied. EPR studies were carried out with enzyme containing natural selenium or with enzyme enriched in ^{77}Se. Samples were prepared with either CO or ^{13}CO. In the Ni_a(I)·CO state, the nuclear spins of both ^{77}Se (I = 1/2) and ^{13}C (I = 1/2) interacted with the nickel-based unpaired electron, suggesting that they are positioned on opposite sites of the nickel ion. In the light-induced signal, the interaction with ^{13}CO was lost. The ^{77}Se nuclear spin introduced an anisotropic hyperfine splitting in both the dark and light-induced EPR signals. The data on the active enzyme of *M. voltae* are difficult to reconcile with the crystal structure of the inactive hydrogenase of *Desulfovibrio gigas* (Volbeda, A., Charon, M. H., Piras, C., Hatchikian, E. C., Frey, M., and Fontecilla Camps, J. C. (1995) *Nature* 373, 580–587) and suggest a structural change in the active site upon activation of the enzyme.

Hydrogenases catalyze the heterolytic cleavage of molecular hydrogen into a hydride and a proton (1, 2), and the oxidation of the hydride to a proton and two electrons. The protons are released, and the electrons are transferred to an electron acceptor. Hydrogenases also catalyze the reverse reaction. All hydrogenases, which can activate hydrogen in the absence of added cofactors, contain transition metals as essential components. On the basis of their amino acid sequences and metal contents, hydrogenases can be divided into two classes. One class consists of enzymes containing only iron. These enzymes are called Fe-hydrogenases or Fe-only hydrogenases (3). The Fe-hydrogenases contain at least two classical (4Fe-4S) clusters (4, 5), in addition to a special cluster involving 4–7 Fe atoms (6), originally proposed to be a novel 6Fe cluster forming the hydrogen-activating site (H-cluster) (7, 8).

The second class comprises hydrogenases containing nickel in addition to iron. These enzymes are called Ni-hydrogenases (also Ni-Fe or [NiFe] hydrogenases). The nickel ion is essential for activity (9, 10). It responds to changes in the redox potential (11–13) and is generally believed to be the heart of the active site (for review, see Ref. 14). Some Ni-hydrogenases contain selenium in the form of selenocysteine (15–17) and are often called [NiFeSe] hydrogenases. They were earlier considered to be a subclass of the Ni-hydrogenases. Comparison of the amino acid sequences (18), however, shows that the basic unit of all known Ni-hydrogenases is the same (14) and the only difference in the Se-containing enzymes is a replacement of a conservative Cys residue by a Sec[1] residue (17).

Depending on the redox potential, the nickel ion can have an unpaired electron. Consequently, nickel hydrogenases have been intensively studied by EPR spectroscopy. Most hydrogenases, when aerobically purified, show two distinct EPR signals due to Ni(III), often within the same preparation. The major difference in the EPR signals is the position of the g_y line of the rhombic signal: it can be either at $g = 2.24$ or at $g = 2.16$ (the g_x lines around 2.3 and the g_z lines around 2.0 differ only slightly). Fernandez *et al.* (19) discovered that enzyme preparations showing a Ni(III) signal with a g_y value of 2.16 were activated by hydrogen within a few minutes, but that several hours were required to activate enzyme molecules with Ni(III) showing a g_y line at 2.24. The states were termed termed "ready" and "unready," respectively. Complete reduction resulted in an active enzyme. In this paper, nickel in ready and unready enzyme will be referred to as Ni_r and Ni_u, respectively. In the literature these states have been called Ni-a and Ni-b (20) or Ni-B and Ni-A (21), respectively. Nickel in active enzyme is called Ni_a. It must be remembered that both the ready and unready enzymes are still inactive and need a reductive activation.

During reductive redox titrations, the $S = 1/2$ EPR signals of Ni(III) disappear and EPR-silent intermediates are obtained (22), in which the nickel ion is considered to be in the divalent, diamagnetic state (14). At temperatures below 10 °C the enzyme remains inactive (23). Only after a reductive treatment at elevated temperatures can the enzyme become active, and only then is it possible to further reduce the divalent nickel ion. This leads to another $S = 1/2$ EPR signal with g values of 2.19, 2.14, and 2.02 (13, 19, 21, 22, 24, 25). As this signal was the third EPR signal from nickel in hydrogenases, it is often called Ni-C. It corresponds to an active state of the enzyme. In the Se-containing enzyme from *Desulfovibrio baculatus*, this state has slightly different g values (2.23, 2.17, and 2.01) (26). This signal is maximal in enzyme under 1% H_2 (27) and then represents about 55% (pH 8–9) to 90% (pH 6) of the nickel concentration. Complete reduction under 200 kPa of H_2 leads to a loss of this EPR signal.

Van der Zwaan *et al.* (25) discovered that the species responsible for this signal in the *Chromatium vinosum* enzyme is light-sensitive at temperatures below 77 K and proposed that this photodissociation involves the breakage of a bond between monovalent nickel and some form of hydrogen. The correspond-

* This work was supported by the Deutsche Forschungsgemeinschaft and Fond der Chemischen Industrie. The costs of publication of this article were defrayed in part by the payment of page charges. This article must therefore be hereby marked "*advertisement*" in accordance with 18 U.S.C. Section 1734 solely to indicate this fact.

§ To whom correspondence should be addressed: Molecular Genetics, Dept. of Biology, University of Marburg, Karl-von-Frisch-Strasse, D-35032 Marburg/Lahn, Germany. Tel.: 49-6421-283247; Fax: 49-6421-286812; E-mail: oliver@molgen.biologie.uni-marburg.de.

[1] The abbreviations used are: Sec, selenocysteine; mT, millitesla.

ing state of nickel will be denoted here as $Ni_a(I)\cdot H_2$ (or Ni-C). Illumination of this state with white light resulted in an EPR spectrum with the lowest g value at 2.05. When performed in D_2O, the rate of photodissociation was nearly 6 times slower and the EPR lines before illumination were slightly sharper (maximally 0.5 mT) than in H_2O. After photodissociation the EPR lines were equally sharp in H_2O and D_2O. In this report the photoproduct of the $Ni_a(I)\cdot H_2$ state will be referred to as $Ni_a(I)[H_2]$.

It has been reported that treatment of Ni-hydrogenases in the most reduced state (under 200 kPa of H_2, here called the $Ni_a(0)$ state) with the competitive inhibitor CO leads to yet another EPR signal (28, 29). The CO-induced species $Ni_a(I)\cdot CO$ was also light-sensitive (28). Illumination resulted in an EPR signal virtually identical to that obtained after illumination of the $Ni_a(I)\cdot H_2$ state. Hence it was ascribed to a $Ni_a(I)[CO]$ state. Indeed, when prepared with ^{13}CO, a nearly isotropic 2-fold splitting of the EPR signal was obtained due to the $I = 1/2$ spin of the ^{13}C nucleus (30). No effect of ^{13}C on the spectrum was observed after illumination. Likewise, no effects of replacement of H_2O by D_2O, neither on the line widths nor on the rate of photodissociation, could be observed in this case. The authors concluded that hydrogen and CO can apparently bind to nickel at the same position, resulting in different EPR spectra in the dark, but identical spectra after photodissociation. As the EPR of the $Ni_a(I)\cdot{}^{13}CO$ species clearly showed an interaction between the unpaired spin of the nickel and the ^{13}CO nucleus (30), the question arose as to why bound hydrogen only gave a slight line broadening, although the proton is a much stronger magnet than ^{13}C.

More recently, we have reported (31) that the anaerobically purified selenium-containing F_{420}-nonreducing hydrogenase from *M. voltae* also displays a light-sensitive EPR signal with all the characteristics of the $Ni_a(I)\cdot H_2$ state (unpaired electron in an orbital with a predominantly d_z2 character). With ^{77}Se-enriched enzyme, an anisotropic splitting due to the $I = 1/2$ nuclear magnetic moment of the isotope was observed, which was 5.3 mT in the z direction, but much smaller (about 0.96 and 1.49 mT) in the x and y directions. After photodissociation of bound hydrogen, the resulting EPR signal (lowest g value at 2.05, so unpaired electron no longer in a d_z2 orbital) showed a nearly isotropic splitting due to ^{77}Se. A reasonable way to explain these data was to assume a 90° flip of the electronic z-axis upon photodissociation. No effects on the line widths could be observed when experiments were performed in D_2O. This means that in the $Ni_a(I)\cdot H_2$ state the unpaired spin in a d_z2 orbital is pointing to Se, but not to hydrogen. Consequently, it was concluded that hydrogen could be bound perpendicular to the Ni-Se axis. Since it is assumed that CO and hydrogen bind to the same site (30), such a proposal can be checked by studying the $Ni_a(I)\cdot{}^{13}CO$ state in the Se-enzyme.

In this contribution we describe the EPR properties of CO-treated selenium-containing F_{420}-nonreducing hydrogenase from *M. voltae*. We have used normal or ^{77}Se-enriched enzyme treated with normal CO or ^{13}CO to further investigate the interactions of the unpaired electron of the nickel center. In addition, we have investigated whether there is a pH effect on the anisotropy of the splitting caused by ^{77}Se in the $Ni_a(I)\cdot H_2$ species. The results are discussed in light of the recent finding that the active site of [NiFe] hydrogenases is a bimetallic complex containing iron and nickel (32, 33).

EXPERIMENTAL PROCEDURES

Growth of M. voltae—M. voltae PS (DSM 1537) was grown at 37 °C in 10-liter batch cultures with a H_2/CO_2 (80:20) gas phase. A small amount of H_2S was added to the gas phase. Cells were harvested anaerobically during late exponential growth, frozen in liquid nitrogen, and stored at −80 °C. A medium according to Whitman *et al.* (34) was used with the following modifications. Cysteine and sodium sulfide were omitted. H_2S was used as a reductant and the sulfur source. Selenite, either the natural isotope mixture or ^{77}Se-derived, was added to a final concentration of 1 μM.

Isotopes—^{77}Se (92.4 atom %) was obtained from Promochem (Wesel, Germany). For oxidation to selenite, the elementary selenium was dissolved in concentrated nitric acid to give a 1 M solution. This solution was used to obtain 1 μM final concentration of selenite in the medium. The selenium concentration in the medium without selenite addition was lower than 3 nM as determined by hydride atomic absorption spectroscopy (Biodata, Linden, Germany). On this basis the ^{77}Se enrichment was calculated to be 92%. ^{13}CO (99 atom %) was obtained from ICN (Eschwege, Germany). To ensure that the CO used was free of traces of oxygen, 0.1 ml of an anaerobic solution of glucose (200 mM in 50 mM Tris/HCl, pH 7.5) and glucose oxidase per milliliter gas volume was added to the gas vessel.

Sample Preparation—Hydrogenase was purified as previously reported (17). Enzyme solutions were concentrated by ultrafiltration through Centricon 30 microconcentrators (Amicon, Witten-Herdecke). This concentrated hydrogenase solution was anaerobically transferred into an EPR tube. The gas atmosphere in the EPR tube was replaced by 100% hydrogen by repeated evacuation and subsequent flushing with hydrogen. Afterward, the sample was incubated for 30 min at 0 °C. The gas atmosphere was then adjusted to 10% CO/90% H_2 by injection of the appropriate volume of CO into the EPR tube, and the tube was then kept at 0 °C for 2.5 min. During this time good equilibrium with the gas phase was promoted by flicking the EPR tube. Subsequently the tube was quickly frozen. As with *C. vinosum* hydrogenase (28), only about one quarter of the enzyme molecules could be converted to the $Ni_a(I)\cdot CO$ state and the EPR signal disappeared if hydrogen was completely replaced by CO.

EPR Spectroscopy—EPR spectra at X band (9 GHz) were obtained with a Bruker ECS 106 EPR spectrometer at a field-modulation frequency of 100 kHz. Cooling of the sample was performed with an Oxford Instruments ESR 900 cryostat with a ITC4 temperature controller. The magnetic field was calibrated with an AEG magnetic field meter. The X-band frequency was measured with a HP 5350B microwave frequency counter. Illumination of the samples was carried out in the helium cryostat by shining white light (Osram Halogen Bellaphot, 150 watts) via a light guide through the irradiation grid of the Bruker ER 4102 ST cavity. Dark adaption of illuminated samples was carried out by placing the samples for 10 min in cold (200 K) ethanol in the dark. For computer simulations, the program EPR (35) or programs of S. P. J. Albracht (36) were used. Normalized double-integral values (*i.e.* the spin concentrations) of the simulated spectra were calculated and used to determine the weights necessary for the simulation of the various spectra.

RESULTS

The $Ni_a(I)\cdot CO$ and $Ni_a(I)[CO]$ States

After reduction and treatment with CO, the hydrogenase from *M. voltae* yielded the EPR spectrum shown in Fig. 1, *trace A*. The most prominent EPR line at $g = 2.11$ is the g_{xy} line of an apparently axial signal, which proved to be light-sensitive and was attributed to the $Ni_a(I)\cdot CO$ species. The g_z line of this signal is expected to be around $g = 2.02$ (28, 29), but was hidden under additional lines originating from reduced Fe-S clusters (lines below $g = 2.05$) and radical species (line around $g = 2$) in the sample. Illumination of the sample led to the disappearance of the feature at $g = 2.11$. The illuminated sample exhibited lines with g values at 2.33 (plus a shoulder at 2.32), 2.28, 2.12, and 2.05, in addition to the lines of Fe-S clusters and radicals (Fig. 1*B*). The photodissociation could be reversed by warming of the sample to 200 K for 10 min in the dark. A difference spectrum, "dark" minus "light" is shown in Fig. 1*C*. This enabled us to observe the changes of the light-sensitive $Ni_a(I)$ species only. Since the gas atmosphere of the sample was a mixture of H_2 and CO, a remainder of the $Ni_a(I)\cdot H_2$ signal could sometimes be observed at g-values of 2.21 and 2.15 (compare *trace C* and *trace D* in Fig. 1). *Trace D* is the difference spectrum of the dark minus light spectrum of the enzyme as isolated under 5% H_2. A comparison of *traces A* and *B* with *trace D* shows that the lines at $g = 2.21$ and $g = 2.15$ are due to the $Ni_a(I)\cdot H_2$ form and the line at $g = 2.28$ and part of the

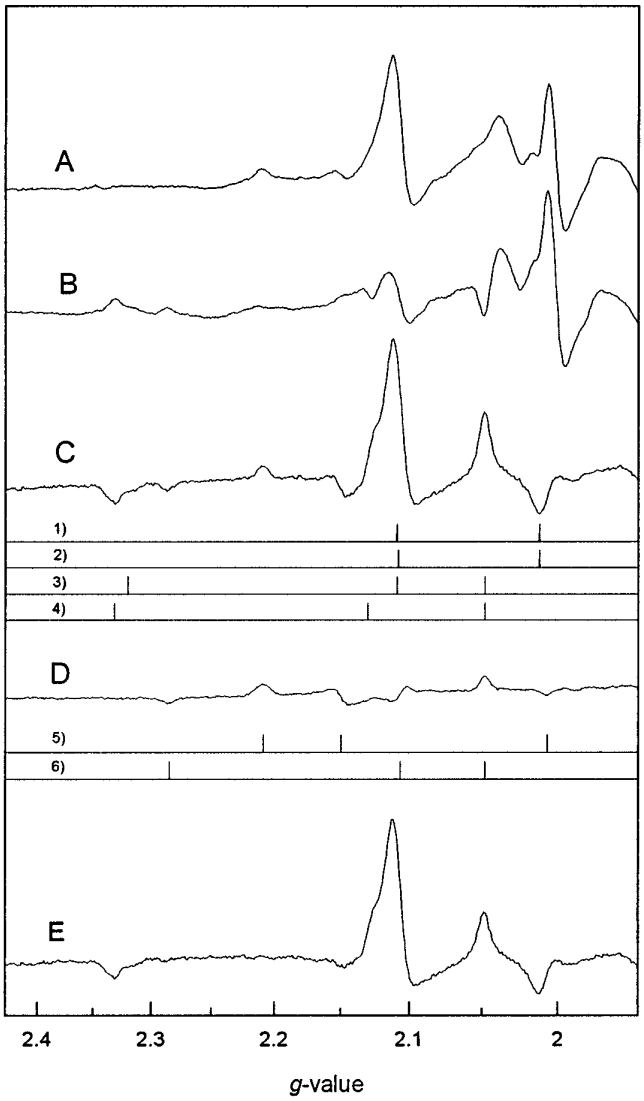

FIG. 1. **EPR spectra of the $Ni_a(I)$·CO state of the *M. voltae* hydrogenase in the dark and after illumination.** Only that part of the spectrum is shown were the nickel species are present. *A*, the $Ni_a(I)$·CO form in the dark. *B*, the $Ni_a(I)[CO]$ form as obtained after 5 min illumination at 70 K with white light. The illumination was continued during the measurement. *C*, difference spectrum of *A* minus *B*. *D*, difference spectrum of the $Ni_a(I)$·H_2 form minus the $Ni_a(I)[H_2]$ form of the enzyme under 5% H_2. *E*, difference spectrum of *C* minus *D*. The *bars* labeled *1–6* indicate the *g* values of the several signals recognized upon analysis (see "Results"). *1*, $Ni_a(I)$·CO-dark-1 species; g_{xyz} = 2.1094, 2.1094, and 2.0123. *2*, $Ni_a(I)$·CO-dark-2 species; g_{xyz} = 2.1084, 2.1084, and 2.0123. *3*, $Ni_a(I)[CO]$-light-1 species; g_{xyz} = 2.0484, 2.1090, and 2.3200. *4*, $Ni_a(I)[CO]$-light-2 species; g_{xyz} = 2.0484, 2.1303, and 2.3315. *5*, $Ni_a(I)$·H_2; g_{xyz} = 2.21, 2.15, and 2.01. *6*, $Ni_a(I)[H_2]$; g_{xyz} = 2.05, 2.11, and 2.28. EPR conditions: microwave frequency, 9420.0 MHz; microwave power, 6.53 milliwatts; modulation amplitude, 1.27 mT; temperature, 70 K.

line at g = 2.11, as well as part of the line at g = 2.05, are due to the $Ni_a(I)[H_2]$ form. The EPR spectrum of the $Ni_a(I)[CO]$ state consists of lines around g = 2.33, 2.12, and 2.05. The bars in the spectrum indicate the g positions of the several signals as determined by computer simulations (see below). In *trace E*, a difference of the spectra shown in *trace C* and *D* is displayed. In this spectrum, the signals of the $Ni_a(I)$·CO and $Ni_a(I)[CO]$ species can be clearly observed.

The $Ni_a(I)$·H_2 and $Ni_a(I)[H_2]$ States

EPR spectra of ^{77}Se-enriched Se-containing hydrogenases have shown that this element is a ligand to nickel (26, 31). The

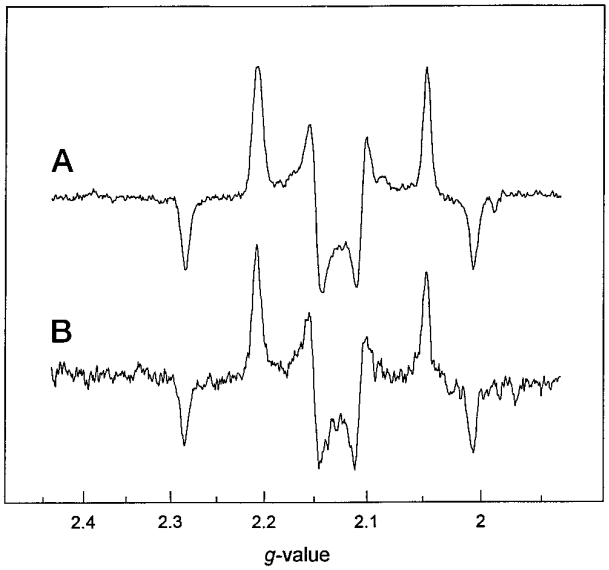

FIG. 2. **Comparison of difference spectra ($Ni_a(I)$·H_2 minus $Ni_a(I)[H_2]$) of samples prepared in H_2O and D_2O.** *A*, difference spectrum of a sample dissolved in H_2O. *B*, difference spectrum of a sample dissolved in D_2O. EPR conditions: microwave frequency, 9424.4 MHz; microwave power, 26 milliwatts; modulation amplitude, 0.638 mT; temperature, 35 K.

observed interactions of the nickel-based unpaired electron with the ^{77}Se nuclear magnetic moment (31) opened the possibility to use the Ni-Se axis as an internal reference frame. This already led to the conclusion (31) that in the $Ni_a(I)$·H_2 state, the bound hydrogen cannot be present as a ligand to nickel in a position opposite to Se, since spectra recorded with a sample in D_2O were not distinguishable from those prepared in H_2O. As this is an important observation in the frame of the discussion in this paper, we show the spectra in Fig. 2.

The $Ni_a(I)$·^{13}CO and $Ni_a(I)[^{13}CO]$ States

Carbon monoxide enriched in ^{13}C had a prominent effect on the EPR spectrum of the $Ni_a(I)$·CO species in the *C. vinosum* enzyme (30), showing that the electronic *z*-axis was along the Ni-CO bond. As outlined in the Introduction, it was assumed that H_2 and CO could bind to the same position. This raised the question why bound ^{13}CO caused a strong hyperfine splitting, whereas bound hydrogen had only a minor effect. To further address this problem, we have investigated the binding of CO and ^{13}CO to active Se-containing *M. voltae* enzyme with and without ^{77}Se. Both ^{77}Se and ^{13}C have a nuclear spin of I = 1/2 and can introduce a 2-fold splitting of the nickel EPR signals if the free electron is interacting with the magnetic ligand. This effect is expected to be considerable if the orbital containing the unpaired spin is pointing toward the ligands.

Fig. 3 displays the spectra obtained with a sample treated with ^{13}CO. In *trace A*, the dark ($Ni_a(I)$·^{13}CO) spectrum is shown. Comparison with Fig. 1*A* shows that the g_{xy} line at g = 2.11 apparently undergoes a 2-fold splitting (2.0 mT) caused by the introduction of the ^{13}C nuclear spin. This points to an interaction between the nuclear spin of the ^{13}C nucleus and the unpaired electron of the nickel. *Trace B* shows a spectrum recorded after illumination of the same sample in the cavity. Although this light ($Ni_a(I)[^{13}CO]$) signal is rather anisotropic, one can detect the low-field features around g = 2.33 and the high-field line at g = 2.05. Theses lines show neither hyperfine splitting nor line broadening (compare Fig. 1*B*). This indicates that after illumination there is no longer an interaction between the unpaired electron of the nickel and the nuclear spin of the ^{13}C, in line with the assumption that illumination leads

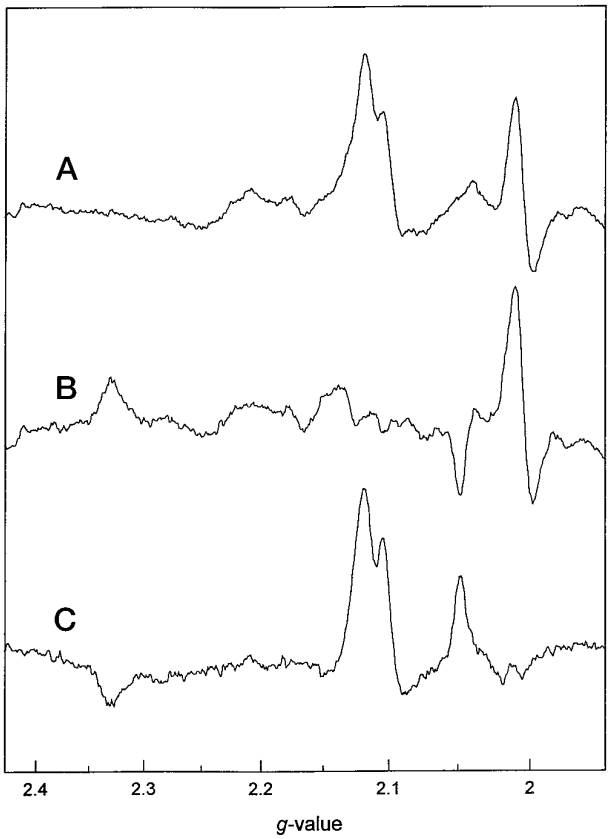

FIG. 3. **EPR spectra of the $Ni_a(I)\cdot^{13}CO$ state of the *M. voltae* hydrogenase in the dark and after illumination.** *A*, the $Ni_a(I)\cdot^{13}CO$ form in the dark. *B*, the $Ni_a(I)[^{13}CO]$ form as obtained after 5-min illumination at 70 K with white light. The illumination was continued during the measurement. *C*, difference spectrum of *A* minus *B*. For the EPR conditions, see Fig. 1.

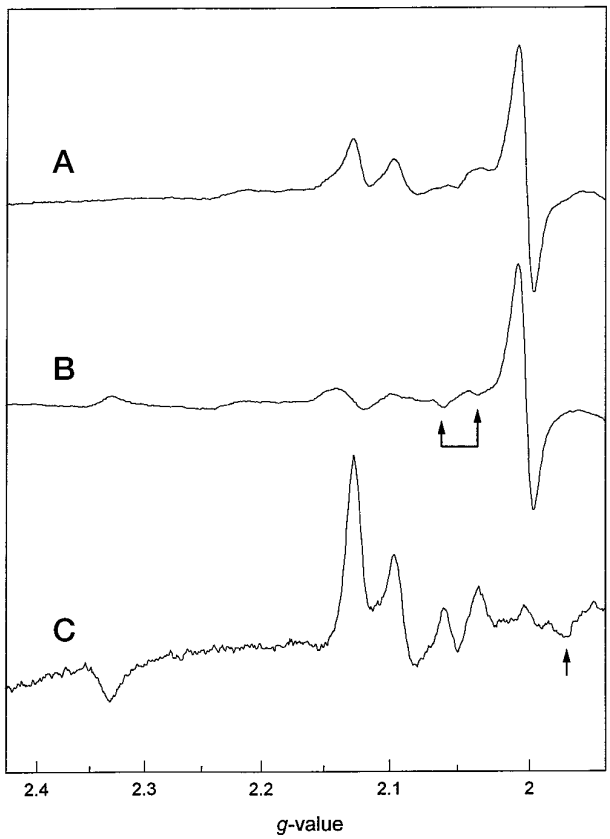

FIG. 4. **EPR spectra of the $Ni_a(I)\cdot CO$ state of ^{77}Se-enriched *M. voltae* hydrogenase in the dark and after illumination.** *A*, the $Ni_a(I)\cdot CO$ form in the dark. *B*, the $Ni_a(I)[CO]$ form as obtained after 5 min illumination at 70 K with white light. The illumination was continued during the measurement. The *arrows* point to the split high-field line. *C*, difference spectrum of *A* minus *B*. The *arrow* indicates the position were a member of the split g_z line of the $Ni_a(I)\cdot CO$ can be detected. For the EPR conditions, see Fig. 1.

to photolysis of the Ni-CO bond. *Trace C* displays the difference spectrum dark minus light. Comparison with Fig. 1*E* indicates that the g_z line of the $Ni_a(I)\cdot^{13}CO$ signal around $g = 2.01$ is split by ^{13}C as well. This region of the spectrum might be somewhat less reliable because the sharp feature in the dark and light spectra can cause some artifacts in the difference spectrum. It can also be seen that the highest g value of the $Ni_a(I)[CO]$ state is at 2.33, whereas the highest g value of the $Ni_a(I)[H_2]$ state (Fig. 1*D*) is at 2.285. This is unlike the situation observed in the *C. vinosum* enzyme (25, 30).

The Effect of ^{77}Se Enrichment

A sample enriched in ^{77}Se and treated with CO yielded a spectrum as shown in Fig. 4. *Trace A* displays the dark spectrum. Here a 2-fold splitting (4.6 mT) of the g_{xy} line at $g = 2.11$ can be observed, indicating an interaction between the unpaired electron of the nickel and the nuclear spin of the ^{77}Se. The g_z line at 2.01 is hidden under signals from Fe-S and radical species in the sample. After illumination of the sample, the spectrum shown in *trace B* was obtained. The splitting introduced by the ^{77}Se nuclear spin is well resolved in the high-field line at $g = 2.05$ (see *arrows*), but apparently not in the low-field lines. Thus also after illumination the ^{77}Se nucleus still interacts with the unpaired electron of the nickel. The difference spectrum of the dark minus light spectrum is displayed in *trace C*. In this spectrum, a splitting of the g_z line of the light-induced signal at $g = 2.05$ can be seen more clearly (compare Fig. 1*E*). The feature observed around $g = 1.98$ (Fig. 4*C*, *arrow*) is most likely a member of the split g_z line of the dark signal, as has become evident from analysis of the spectra with the help of simulations (see below and Table I). The splittings caused by ^{77}Se in the $Ni_a(I)\cdot CO$ signal appear rather anisotropic (see below). As before, the region around $g = 2$ might be less reliable due to the strong radical signals in the parent spectra.

Effect of pH

As mentioned in the Introduction, an anisotropic splitting due to ^{77}Se was observed in ^{77}Se-enriched samples in the $Ni_a(I)\cdot H_2$ state. This could have been an effect of partial protonation of the selenol group. It has been speculated that this group might serve as a basic group, which could bind the proton originating from the heterolytic cleavage of H_2. In this case the shape of the spectrum might be expected to change with changing pH. This notion was tested by taking spectra of ^{77}Se-enriched samples in the $Ni_a(I)\cdot H_2$ state in the range of pH 6 to 9 (Fig. 5). In this range no changes in the spectra were observed.

Computer Simulation

The data in Figs. 1, 3, and 4 show that in the dark state the unpaired electron of nickel interacts with both the ^{77}Se nucleus and the ^{13}C nucleus of CO. After illumination interaction with the ^{13}C nucleus was lost. In contrast, the ^{77}Se nucleus still interacted with the unpaired spin after illumination.

To verify this interpretation and to more precisely determine the g values and hyperfine tensors, simulations of the experimental spectra were made. Where necessary, the contributions to the spectra of the $Ni_a(I)\cdot H_2$ and $Ni_a(I)[H_2]$ species were

TABLE I

Parameters used for the simulation of the EPR spectra of F_{420}-nonreducing hydrogenase (Approach I)

The table gives the *g* values, line widths and hyperfine-splitting values used for simulation of different signals. The line width (*W*) in mT is defined for the absorption type peaks as the half-line width at half-height and for the derivative type as the half peak-to-peak distance.

Signal	*g* values			Line width (mT)			Hyperfine splitting (mT)		
	g_x	g_y	g_z	W_x	W_y	W_z	A_x	A_y	A_z
Dark 1									
CO/Se	2.1094	2.1094	2.0123	2.588	2.588	1.248	—	—	—
^{13}CO/Se							1.21	1.21	1.75
CO/^{77}Se							3.90	3.90	11.76
Dark 2									
CO/Se	2.1084	2.1084	2.0123	1.023	1.023	1.248	—	—	—
^{13}CO/Se							2.26	2.26	1.75
CO/^{77}Se							4.68	4.68	11.76
Light 1									
CO/Se	2.0484	2.1090	2.3200	0.900	1.200	1.598	—	—	—
CO/^{77}Se							3.49	7.39	0.95
Light 2									
CO/Se	2.0484	2.1303	2.3315	0.900	0.600	0.618	—	—	—
CO/^{77}Se							3.49	1.30	1.01

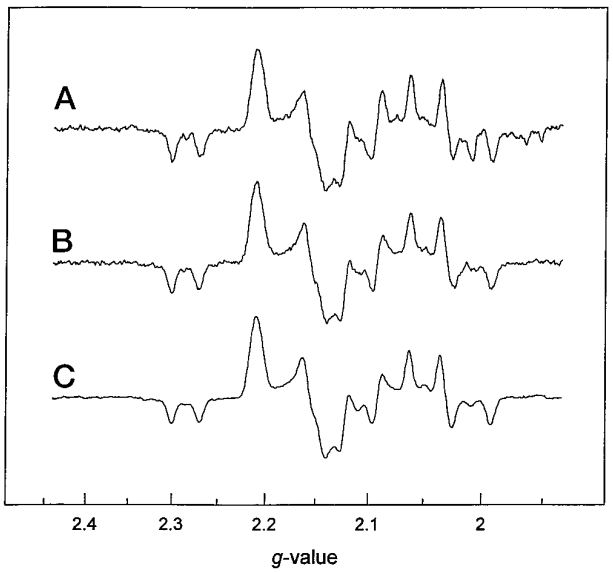

FIG. 5. **Comparison of the ^{77}Se hyperfine splitting in EPR signals of samples in the $Ni_a(I)\cdot H_2$ state at different pH values.** Displayed are difference spectra of $Ni_a(I)\cdot H_2$ minus $Ni_a(I)[H_2]$. *A*, sample at pH 6. *B*, sample at pH 7.5. *C*, sample at pH 9. For EPR conditions see Fig. 2.

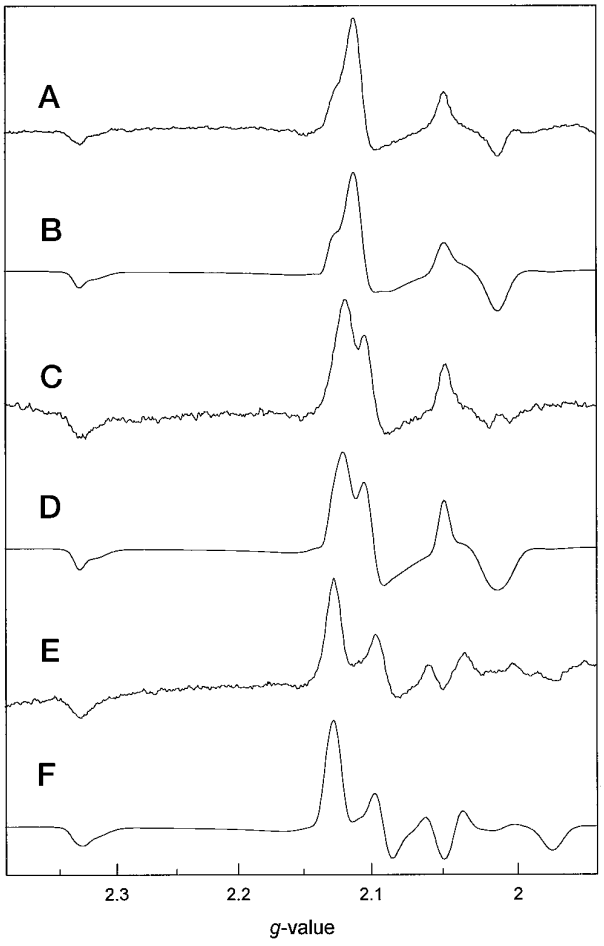

FIG. 6. **Comparison of the difference spectra from Figs. 1–3 with the corresponding simulated spectra using simulation approach I.** *A*, $Ni_a(I)\cdot CO$ minus $Ni_a(I)[CO]$ (same as Fig. 1*E*). *B*, simulation of *A*. *C*, $Ni_a(I)\cdot^{13}CO$ minus $Ni_a(I)[^{13}CO]$ (same as Fig. 3*C*). *D*, simulation of *C*. *E*, as in *A* but prepared from ^{77}Se-enriched hydrogenase (same as Fig. 4*C*). The parameters and relative intensities used for the simulations are shown in Tables I and II, respectively.

subtracted. Dark minus light difference spectra as in Fig. 1*D* (or from a ^{77}Se-enriched sample) were used for this purpose. In view of the limited quality of the EPR spectra, resulting from the limited amounts of isotope-enriched enzyme and overlapping Fe-S, radical, and other background signals (Figs. 1, 3, and 4), two different approaches for computer simulations were applied.

Approach I—In this approach, the line shapes of the dark minus light difference spectra were obtained after conversion of all spectra to the same microwave frequency (9420 MHz). It was assumed that features below $g = 2.03$ in the difference spectra were not very reliable due to sharp lines in the parent spectra. Simulation were performed with the program of F. Neese (35).

Comparisons of experimental and simulated spectra are shown in Fig. 6. The $Ni_a(I)\cdot CO$ signal was best simulated as the sum of two axial signals with slightly different g_{xy} values, but with considerably different W_{xy} values. In addition, the $Ni_a(I)[CO]$ spectrum was simulated as a sum of two different rhombic signals. For each simulation, the enrichment in ^{77}Se was taken into account (7.58% for normal samples and 92% for the ^{77}Se-enriched samples). Hence, every simulated difference spectrum consisted of a sum of eight signals. The EPR parameters of these eight spectra are summarized in Table I, and the relative intensities, used to compose the spectra in Fig. 6 (*traces B*, *D*, and *F*) are given in Table II. Note that the ratio of the two dark signals equals the ratio of the two light-induced signals. Using this approach, it thus seems that two slightly different species of the $Ni_a(I)\cdot CO$ form were present. It was

TABLE II

Relative intensities (%), based on g value-normalized double-integral values, of the individual spectra used to compose the simulations of Fig. 6, traces B, D, and F

The simulation parameters are shown in Table I. As can be seen the natural abundance of ^{77}Se (7.58%) was taken into account for the samples not enriched in this isotope. The effects upon the spectra of the natural abundance of ^{13}C (1.1%) was neglected.

Trace	Dark 1				Dark 2			
	CO/Se	CO/^{77}Se	^{13}CO/Se	^{13}CO/^{77}Se	CO/Se	CO/^{77}Se	^{13}CO/Se	^{13}CO/^{77}Se
B	58.81	4.82			33.61	2.76		
D			58.81	4.82			33.61	2.76
F	5.09	58.55			2.91	33.45		
Trace	**Light 1**				**Light 2**			
	CO/Se	CO/^{77}Se	^{13}CO/Se	^{13}CO/^{77}Se	CO/Se	CO/^{77}Se	^{13}CO/Se	^{13}CO/^{77}Se
B	−58.81	−4.82			−33.61	−2.76		
D	−58.81	−4.82			−33.61	−2.76		
F	−5.09	−58.55			−2.91	−33.45		

noted that the ratio of these forms was constant in all simulations of spectra of several different samples. As can be seen in Fig. 6, the simulated spectra fitted quite well in the region above $g = 2.03$, but below that value too much intensity was obtained for the g_z line of the $Ni_a(I)$·CO signal.

Approach II—Here it was assumed that, like in our previous studies on the $Ni_a(I)$·H_2 state (31), the region below $g = 2.03$ was also a reliable representation of the EPR line shapes of the $Ni_a(I)$·CO and $Ni_a(I)$·[CO] states. For an overall comparison, slight differences in experimental microwave frequency among the EPR tube were not corrected. Illumination of a sample did not change this frequency. The programs of S. P. J. Albracht (36) were used.

The $Ni_a(I)$·CO spectrum was simulated as a single axial signal, whereas the spectrum obtained after illumination, the $Ni_a(I)$[CO] state, was an overlap of two signals with different g_z (and W_z) values around $g = 2.33$, but the same g_y and g_x values and widths. Fig. 7 summarizes the results (see also Tables III and IV). Now the features below $g = 2.03$ fitted reasonably well.

DISCUSSION

Conclusions from the Simulations—Simulations according to approach I gave quite good fits, except for the region below $g = 2.03$. Following approach II, much better fits were obtained for this particular region, but now the low-field shoulder around $g = 2.13$ in Fig. 7*A* could not be accounted for. In using approach II, it was noticed that all simulations shown in Fig. 7 differed in the $g = 2.13$ region in the same way from the experimental dark minus light spectra of the three different samples, and hence this difference was not sensitive to ^{13}CO or ^{77}Se. It is presumably due to a light-sensitive change not related to the nickel site. It was this feature that determined whether the spectrum of the $Ni_a(I)$·CO state was simulated as one species (approach II) or two species (approach I). In view of the better overall fits with approach II, we conclude that there is presumably only one $Ni_a(I)$·CO state.

In evaluating both approaches, we come to the following conclusions about the effects of CO, ^{13}CO, and ^{77}Se on the EPR spectra. Like in the *C. vinosum* and *D. gigas* enzymes, CO binds to the nickel site in the *M. voltae* enzyme in a light-sensitive way. The $Ni_a(I)$·CO state is presumably homogeneous as in the other enzymes, whereas in the $Ni_a(I)$[CO] state two major components can be detected by EPR. Unlike the situation in the *C. vinosum* hydrogenase, the $Ni_a(I)$[CO] state has an EPR spectrum differing from that of the $Ni_a(I)$[H_2] state. Reaction of the enzyme with ^{13}CO results in a nearly isotropic interaction (A_{xyz} = 2.2, 2.2, and 2.35 mT) in the $Ni_a(I)$·^{13}CO state. Enrichment with ^{77}Se gives rise to A_{xyz} = 4.6, 4.6, and 12.1 mT in the $Ni_a(I)$·CO state. After illumination the g_z region

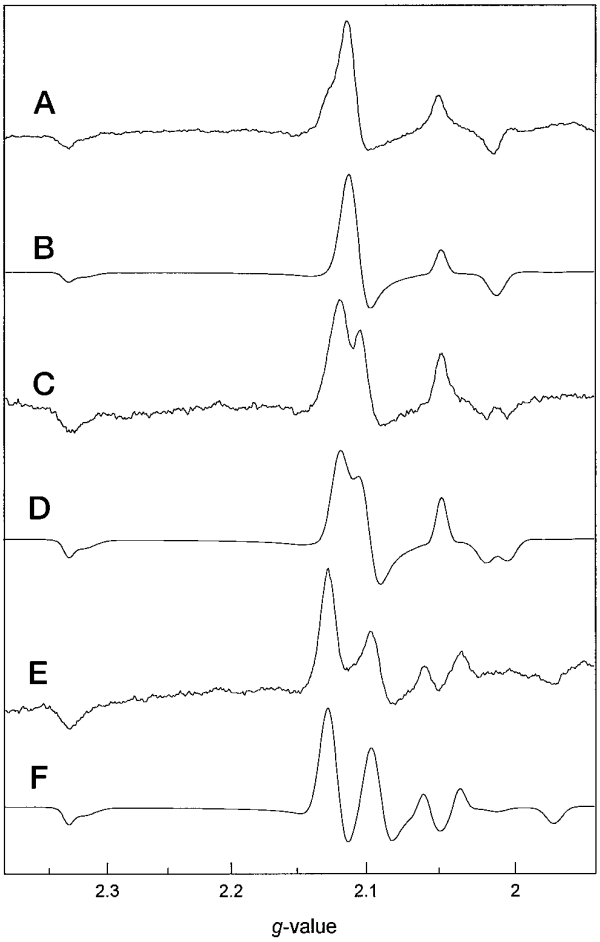

FIG. 7. **Comparison of the difference spectra from Figs. 1–3 with the corresponding simulated spectra using simulation approach II.** *A*, $Ni_a(I)$·CO minus $Ni_a(I)$[CO] (same as Fig. 1*E*). *B*, simulation of *A*. *C*, $Ni_a(I)$·^{13}CO minus $Ni_a(I)$[^{13}CO] (same as Fig. 3*C*). *D*, simulation of *C*. *E*, as in *A* but prepared from ^{77}Se-enriched hydrogenase (same as Fig. 4*C*). The original microwave frequencies of the experimental spectra were used (9420–9421.7 MHz). The *g* scale is given for 9421 Mhz. The parameters and relative intensities used for the simulations are shown in Tables III and IV, respectively.

of the resulting $Ni_a(I)$[CO] signals is indistinguishable from that obtained with the ^{13}CO-treated enzyme. This means that, under the conditions used, the ^{77}Se nucleus has no detectable hyperfine splitting in this direction. The g_x region shows a clear splitting of 3.81 mT. Information on the *g* and *A* values of the g_y region is unreliable due to overlapping background signals and overlap with the *g* region of the $Ni_a(I)$·CO signal. We have assumed common g_y (2.114), W_y (2.7 mT), and A_y values (3.81

TABLE III

Parameters used for the simulation of the EPR spectra of F_{420}-nonreducing hydrogenase (Approach II)

The table gives the *g* values, line widths, and hyperfine-splitting values used for simulation of the different signals. The line width (*W*) in mT is defined as the peak-to-trough width of the derivative Gaussians used for the simulations; for absorption-type lines this is the width at the inflection points, and for the derivative-type lines this is the peak-to-trough width.

Signal	*g* values			Line width (mT)			Hyperfine splitting (mT)		
	g_x	g_y	g_z	W_x	W_y	W_z	A_x	A_y	A_z
Dark									
CO/Se	2.1084	2.1084	2.0123	2.05	2.05	1.7	—	—	—
^{13}CO/Se							2.2	2.2	2.35
CO/^{77}Se							4.6	4.6	12.1
Light 1									
CO/Se	2.0484	2.1137	2.3200	1.2	2.7	2.68	—	—	—
CO/^{77}Se							3.81	3.81	0
Light 2									
CO/Se	2.0484	2.1137	2.3315	1.2	2.7	1.04	—	—	—
CO/^{77}Se							3.81	3.81	0

TABLE IV

Relative intensities (%), based on g value-normalized double-integral values, of the individual spectra used to compose the simulations of Fig. 7, traces B, D, and F

The EPR parameters are in Table III. As can be seen the natural abundance of ^{77}Se (7.58%) was taken into account for the samples not enriched in this isotope. The effects upon the spectra of the natural abundance of ^{13}C (1.1%) was neglected.

Trace	Dark			
	CO/Se	CO/^{77}Se	^{13}CO/Se	^{13}CO/^{77}Se
B	92.42	7.58		
D			92.42	7.58
F	8.0	92.0		

Trace	Light 1		Light 2	
	CO/Se	CO/^{77}Se	CO/Se	CO/^{77}Se
B	−58.81	−4.84	−33.61	−2.76
D	−58.81	−4.84	−33.61	−2.76
F	−5.09	−58.55	−2.91	−33.45

mT) for the two light-induced signals.

CO Binds to Nickel in a Position Opposite to Se—The *g* values of the $Ni_a(I)$·CO signal (g_z close to g_e and the other *g* values greater than g_z) indicate that the unpaired spin is in an orbital with a predominant d_z2 character (37). The sample treated with ^{13}CO showed a significant and nearly isotropic hyperfine interaction of the unpaired spin of the nickel with the ^{13}C nucleus. This indicates that the d_z2 orbital bearing the unpaired spin is overlapping with the *sp*-hybrid orbital of the carbon atom. It then follows that the CO is a ligand in the direction of the d_z2 orbital (*i.e.* the electronic *z*-axis).

The $Ni_a(I)$·CO spectrum of a ^{77}Se-enriched sample also clearly showed a large hyperfine splitting of all lines, although it was rather anisotropic in nature (A_{xyz} = 4.6, 4.6, and 12.1 mT). This demonstrated that the d_z2 orbital is also pointing toward the selenium atom. These two results indicate that in the CO-treated enzyme, selenium and the carbon atom of the CO are located along the *z*-axis of the *g*-tensor system. We therefore conclude that Se and CO bind on opposite sites to the nickel ion. This means that a flip of 90° of the electronic *z*-axis upon CO binding, as earlier proposed (31), does not take place. Illumination of the $Ni_a(I)$·CO state resulted in a similar, although not identical, EPR spectrum as illumination of the $Ni_a(I)$·H_2 state (31), whereas the hyperfine interactions with ^{77}Se differed considerably (for $Ni_a(I)$·CO: A_{xyz} = 4.6, 4.6, and 12.1 mT; for $Ni_a(I)[CO]$: 3.81, 3.81, and 0 mT; for $Ni_a(I)$·H_2: 0.96, 1.55, and 5.32 mT; for $Ni_a(I)[H_2]$: 4.33, 4.67, and 3.81 mT).

A plausible explanation for the ^{77}Se- hyperfine splitting in all of these states is that the *z*-axis in both dark states (electron in d_z2) is along the Ni-Se axis, but perpendicular to this axis in the light-induced states (electron in $d_{x^2-y^2}$). The differences in ^{77}Se-hyperfine interaction when CO is present points to a difference in orbital overlap between nickel and selenium, probably due to a slightly distorted structure, in line with the difference in *g* values of the $Ni_a(I)[H_2]$ and $Ni_a(I)[CO]$ states.

Comparison of CO Binding and Hydrogen Binding—F_{420}-nonreducing hydrogenase from *M. voltae*, as anaerobically purified in a glove box containing 5% H_2, shows EPR characteristics that are typical for [NiFe] hydrogenases in the $Ni_a(I)$·H_2 state (31) (Fig. 1*D*). Treatment of fully reduced samples with 10% CO resulted in different EPR spectra (Fig. 1*A*). The change of the *g* values upon CO treatment indicates binding of CO to nickel, and this is confirmed by the use of ^{13}CO. We note that the ^{13}C splittings are somewhat smaller than those observed in the $Ni_a(I)$·^{13}CO state of the *C. vinosum* hydrogenase (A_{xyz} = 2.88, 3.04, and 3.2 mT; Ref. 30). The *C. vinosum* enzyme showed a rhombic EPR signal (g_{xyz} = 2.12, 2.07, and 2.02), whereas the signal of the $Ni_a(I)$·CO state from the *M. voltae* enzyme is axial (g_{xyz} = 2.11, 2.11, and 2.01). We also note that the ^{77}Se-hyperfine interaction in the $Ni_a(I)$·CO state (A_{xyz} = 4.6, 4.6, and 12.1 mT) is considerably stronger than in the $Ni_a(I)$·H_2 state (A_{xyz} = 0.96, 1.548, and 5.32 mT) (31).

Illumination at low temperatures of CO-treated *M. voltae* samples led to a spectrum that differed noticeably from that of the $Ni_a(I)$·$[H_2]$ state. The highest *g* value of the former is 2.32 (species 1) to 2.3315 (species 2), whereas the latter has a highest *g* value of 2.285 (Fig. 1.). In this respect the enzymes from *M. voltae* and *C. vinosum* also differ; with the *C. vinosum* enzyme, the *g* values of the $Ni_a(I)[H_2]$ and $Ni_a(I)[CO]$ states were identical. This suggests that the changes in the conformation of the nickel site induced by binding of the H-species (the $Ni_a(I)$·H_2 state) or CO are different in the *M. voltae* enzyme; after photolysis of the added ligands, the EPR spectra differ. In the *C. vinosum* enzyme, the H-species and CO apparently induce the same (if any) conformational changes.

There is a second major difference in EPR properties of the $Ni_a(I)[H_2]$ and $Ni_a(I)[CO]$ states in the *M. voltae* enzyme. In the former state the ^{77}Se-hyperfine interaction is quite isotropic (A_{xyz} = 4.327, 4.665, and 3.81 mT) (31), but in the latter state a strongly anisotropic interaction is observed (A_{xyz} = 3.81, 3.81, and 0 mT). This strengthens the notion that CO binding to the *M. voltae* enzyme perturbs the coordination of the active site more than hydrogen binding.

Based on the assumption that the unpaired electron in the $Ni_a(I)\cdot H_2$ and $Ni_a(I)\cdot CO$ state is in an orbital with mainly a d_z2 character, the results on the Se-containing *M. voltae* enzyme (this paper and Ref. 31) allow the conclusion that in the $Ni_a(I)\cdot H_2$ state there is no hydrogen species bound opposite to selenocysteine, but that the site is empty and available for binding of CO or H_2 (27). This is in agreement with the very small effect of H/D exchange on the line width of the $Ni_a(I)\cdot H_2$ spectra from various hydrogenases (25, 38) including the F_{420}-nonreducing enzyme from *M. voltae* (Fig. 2). It means that the light-sensitive hydrogen species bound to the active site (25, 39, 40) is bound elsewhere. One possibility is binding perpendicular to the *z*-axis as suggested by Marganian *et al.* (41, 42) on the basis of Ni(I) model compounds that had reacted with CO or H_2. Another possibility is binding to Fe in the active [NiFe] site. The present data do not allow us to distinguish between these possibilities.

Illumination of the $Ni_a(I)\cdot H_2$ and the $Ni_a(I)\cdot CO$ states produces identical EPR spectra in *C.vinosum* hydrogenase (30) and similar spectra in the *M. voltae* enzyme. This raises an interesting question: if the photodissociation of the Ni-CO bond is the only light-induced reaction, then why is the EPR spectrum of the $Ni_a(I)$[CO] state (position opposite the Se vacant) completely different from that of the $Ni_a(I)\cdot H_2$ state (likewise having a vacant position opposite the Se site)? Is a light-sensitive hydrogen species still bound to the active site in the $Ni_a(I)\cdot CO$ state? In this respect we note that we have never been able to prepare the $Ni_a(I)\cdot CO$ state in the absence of H_2 in the gas phase, so the possibility that both CO and a hydrogen species are bound in this state, be it at different sites, remains to be tested.

In summary, the results presented in this paper suggest that CO can bind to nickel opposite the selenium atom. There is a large amount of delocalization of the electron density of the nickel-based unpaired spin toward both ligands. In the absence of CO the site opposite selenium is vacant. Our data also suggest that the hydrogen species present in the $Ni_a(I)\cdot H_2$ state might also be present in the $Ni_a(I)\cdot CO$ state. This hydrogen species could be bound perpendicular to the electronic z-axis or to the iron atom. The results in Fig. 5. make a protonation of selenium in the $Ni_a(I)\cdot H_2$ state in the range of pH 6 to 9 unlikely, since there is no change in *g* values or hyperfine interaction. The proton generated upon cleavage of dihydrogen might bind to another ligand.

The present results on an active hydrogenase are difficult to reconcile with the x-ray structure of the oxidized, inactive *D. gigas* enzyme (33). Here the position opposite the sulfur atom, which is analogous to the selenium atom in the *M. voltae* enzyme, is occupied by another sulfur atom. A different structure in active enzyme is in line with the great change in properties of the active site in nickel hydrogenases upon activation/deactivation (14). No x-ray data are available on the active *D. gigas* enzyme yet.

Acknowledgments—S. P. J. A. is indebted to the Netherlands Foundation for Chemical Research, for grants, supplied via the Netherlands Organization for Scientific Research, which enabled the purchase of the Bruker ECS 106 EPR spectrometer.

REFERENCES

1. Krasna, A. L., and Rittenberg, D. (1954) *J. Am. Chem. Soc.* **76,** 3015–3020
2. Rittenberg, D., and Krasna, A. I. (1955) *Disscuss. Faraday Soc.* **20,** 185–189
3. Adams, M. W. W. (1990) *Biochim. Biophys. Acta* **1020,** 115–145
4. Voordouw, G., and Brenner, S. (1985) *Eur. J. Biochem.* **148,** 515–520
5. Meyer, J., and Gagnon, J. (1991) *Biochem.* **30,** 9697–9704
6. Pierik, A. J., Wolbert, R. B. G., Mutsaers, P. H. A., Hagen, W. R., and Veeger, C. (1992) *Eur. J. Biochem.* **206,** 697–704
7. Hagen, W. R., van Berkel-Arts, A., Krüse-Wolters, K. M., Dunham, W. R., and Veeger, C. (1986) *FEBS Lett.* **201,** 158–162
8. Hagen, W. R., van Berkel-Arts, A., Krüse-Wolters, K. M., Voordouw, G., and Veeger, C. (1986) *FEBS Lett.* **203,** 59–63
9. Friedrich, B., Heine, E., Finck, A., and Friedrich, C. G. (1981) *J. Bacteriol.* **145,** 1144–1149
10. Graf, E.-G., and Thauer, R. K. (1981) *FEBS Lett.* **136,** 165–169
11. Albracht, S. P. J., Graf, E.-G., and Thauer, R. K. (1982) *FEBS Lett.* **140,** 311–313
12. Moura, J. J. G., Moura, I., Huynh, B. H., Krüger, H. J., Teixeira, M., DuVarney, R. G. DerVartanian, D. V. Ljungdahl, P., Xavier, A. V. Peck, H. D., Jr., and LeGall, J. (1982) *Biochem. Biophys. Res. Commun.* **108,** 1388–1393
13. Kojima, N., Fox, J. A., Hausinger, R. P., Daniels, L., Orme-Johnson, W. H., and Walsh, C. T. (1983) *Proc. Natl. Acad. Sci. U. S. A.* **80,** 378–382
14. Albracht, S. P. J. (1994) *Biochim. Biophys. Acta* **1188,** 167–204
15. Yamazaki, S. (1982) *J. Biol. Chem.* **257,** 7926–7929
16. Halboth, S., and Klein, A. (1992) *Mol. Gen. Genet.* **233,** 217–224
17. Sorgenfrei, O., Linder, D., Karas, M., and Klein, A. (1993) *Eur. J. Biochem.* **213,** 1355–1358
18. Voordouw, G. (1992) *Adv. Inorg. Chem.* **38,** 397–422
19. Fernandez, V. M., Hatchikian, E. C., and Cammack, R. (1985) *Biochim. Biophys. Acta* **832,** 69–79
20. Albracht, S. P. J., Kalkman, M. L., and Slater, E. C. (1983) *Biochim. Biophys. Acta* **724,** 309–316
21. Teixeira, M., Moura, I., Xavier, A. V., Huynh, B. H., DerVartanian, D. V., Peck, H. D. Jr., LeGall, J., and Moura, J. J. G. (1985) *J. Biol. Chem.* **260,** 8942–8950
22. Teixeira, M., Moura, I., Xavier, A. V., DerVartanian, D. V., LeGall, J., Peck, H. D., Jr., Huynh, B. H., and Moura, J. J. G. (1983) *Eur. J. Biochem.* **130,** 481–484
23. Coremans, J. M. C. C. (1991) *Redox Properties of Hydrogenase.* Ph.D. Thesis, University of Amsterdam, The Netherlands
24. Fernandez, V. M., Hatchikian, E. C., Patil, D. S., and Cammack, R. (1986) *Biochim. Biophys. Acta* **883,** 145–154
25. van der Zwaan, J. W., Albracht S. P. J., Fontijn, R. D., and Slater, E. C. (1985) *FEBS Lett.* **179,** 271–277
26. He, S. H., Teixeira, M., LeGall, J., Patil, D. S., Moura, I., Moura, J. J. G., DerVartanian, D. V., Huynh, B. H., and Peck, H. D., Jr. (1989) *J. Biol. Chem.* **264,** 2678–2682
27. Coremans, J. M. C. C., van Garderen, C. J., and Albracht, S. P. J. (1992) *Biochim. Biophys. Acta* **1119,** 148–156
28. van der Zwaan, J. W., Albracht, S. P. J., Fontijn, R. D., and Roelofs, Y. B. M. (1986) *Biochim. Biophys. Acta* **872,** 208–215
29. Cammack, R., Patil, D. S., Hatchikian, E. C., and Fernandez, V. M. (1987) *Biochim. Biophys. Acta* **912,** 98–109
30. van der Zwaan, J. W., Coremans, J. M. C. C., Bouwens, E. C. M., and Albracht, S. P. J. (1990) *Biochim. Biophys. Acta* **1041,** 101–110
31. Sorgenfrei, O., Klein, A., and Albracht, S. P. J. (1993) *FEBS Lett.* **332,** 291–297
32. Surerus, K. K., Chen, M., Van der Zwaan, J. W., Rusnak, F. M., Kolk, M., Duin, E. C., Albracht, S. P. J., and Münck, E. (1994) *Biochem.* **33,** 4980–4993
33. Volbeda, A., Charon, M. H., Piras, C., Hatchikian, E. C., Frey, M., and Fontecilla Camps, J. C. (1995) *Nature* **373,** 580–587
34. Whitman, W. B., Ankwanda, E., and Wolfe, R. S. (1982) *J. Bacteriol.* **149,** 852–863
35. Neese, F. (1995) Quantum Chemistry Program Exchange, Program No. QCMP 136, Indiana, U. S. A.
36. Beinert, H., and Albracht, S. P. J. (1982) *Biochim. Biophys. Acta* **683,** 245–277
37. Wertz, J. E., and Bolton, J. R. (1972) *Electron Spin Resonance: Elementary Theory and Practical Applications*, McGraw-Hill Book Company, New York
38. Medina, M., Cammack, R., Williams, R., and Hatchikian, E. C. (1994) *J. Chem. Soc. Faraday Trans.* **90,** 2921
39. Fan. C., Teixeira, M., Moura, J., Moura, I., Huynh, B.-H., Le Gall, J., Peck, H. D., Jr., and Hoffman, B. M. (1991) *J. Am. Chem. Soc.* **113,** 20–24
40. Whitehead, J. P., Gurbiel, R. J., Bagyinka, C., Hoffman, B. M., and Maroney, M. J. (1993) *J. Am. Chem. Soc.* **115,** 5629–5635
41. Marganian, C. A., Vazir, H., Baidya, N., Olmstead, M. M., and Mascharak, P. K. (1995) *J. Am. Chem. Soc.* **117,** 1584–1594
42. Marganian-Goldman, C., and Mascharak, P. K. (1995) *Comments Inorg. Chem.* **18,** 1–2